Supporting Information for Publication:

Sub-Picosecond Photodynamics of Small Neutral Copper Oxide Clusters

Chase H. Rotteger,[1,2] Carter K. Jarman,[1,2] Madison M. Sobol,[1,2] Shaun F. Sutton,[1,2] and Scott G. Sayres[1,2,]*

School of Molecular Sciences, Arizona State University, Tempe, AZ 85287

Biodesign Center for Applied Structural Discovery, Arizona State University, Tempe, AZ 85287

UV-Vis Spectra

The UV-Vis spectra are generated from TD-DFT calculations of the copper oxide clusters (presented in Figure S1. As oxidation increases in the cluster series, a higher density of states is present, allowing for faster relaxation. The isodensities for the excited state near 3.1 eV, equivalent to the 400 nm pump photon energy and the optical gap states are presented. The charge carrier densities for the states at 3.1 eV are similar to the optical gap states presented in the main text, with the hole (blue) and electrons (green) generally residing on the same atoms in both situations. The primary difference is which Cu-d orbital acts as the hole.
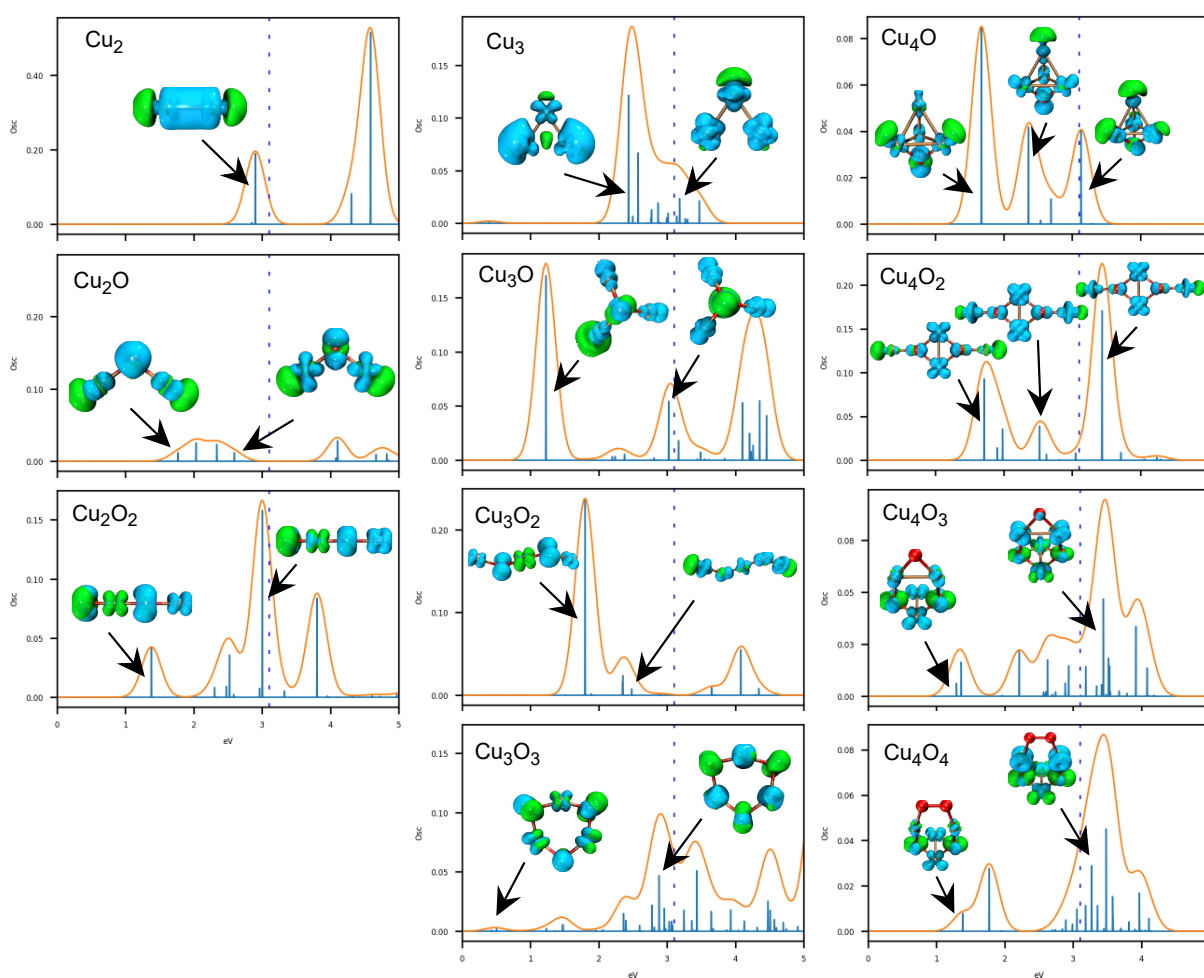

Figure S1. Calculated UV-Vis spectra for the Cu_nO_x (n = 2-4) series. The transition densities calculated for several states are shown with an isodensity of 0.004 /$Å^3$, where the electron is green and hole is blue.

The calculated TDI values for the O_g excited state is similar to the TDI of the excited states near 3.1 eV. The similarity in these values demonstrates that the charge carrier distribution is important for driving relaxation rates, and justifies the approximation of using the optical gap state for the calculations in the main text.

Table S1. The calculated TDI values for the optical gap and 3.1 eV excited states with the percent difference for each cluster calculated.

Cluster	O_g TDI (Å^{-3})	3.1 eV TDI (Å^{-3})	Percent Difference
$^1Cu_2$	1.08	1.08	0.00
$^1Cu_2O$	2.24	2.10	6.40
$^3Cu_2O_2$	2.77	2.60	6.24
$^2Cu_3$	0.89	0.70	23.98
$^2Cu_3O$	0.98	0.84	15.92
$^2Cu_3O_2$	2.90	1.71	51.52
$^4Cu_3O_3$	2.34	2.24	4.30
$^1Cu_4O$	1.36	1.60	16.31
$^1Cu_4O_2$	1.88	1.64	13.51
$^3Cu_4O_3$	3.04	2.18	32.81
$^3Cu_4O_4$	3.19	2.88	10.17

Cation Distribution

The cation distribution (Fig. S2), produced directly from the laser vaporization source, contains similar stoichiometric distributions and size range as the neutral clusters as $(Cu_2O)_n$ is the most prominent stoichiometry. However, as cation cluster size increases, the preferred stoichiometry shifts towards lower oxygen content, where in the neutral clusters the shift is towards more oxidized clusters. Both distributions show a strong peak for Cu_2O, and Cu_3O. However, the cation distribution for Cu_3O_2 and Cu_3O_3 are significant, whereas they are small in the neutral distribution. This aligns with the lower stability noted for oxidized clusters. Similarly, both clusters contain large peak for Cu_5O_3. In particular, the cation distribution contains large signals associated with Cu_4O, and Cu_5O which are absent in the neutral beam. The majority of the clusters are present in both, with varying relative intensity. The Cu_7O_{3-5} series are dominant in both distributions, so is the Cu_8O_{3-5} and Cu_9O_{4-6}. Thus, the SFI clusters likely provides a reasonable representation of the neutral cluster distribution.
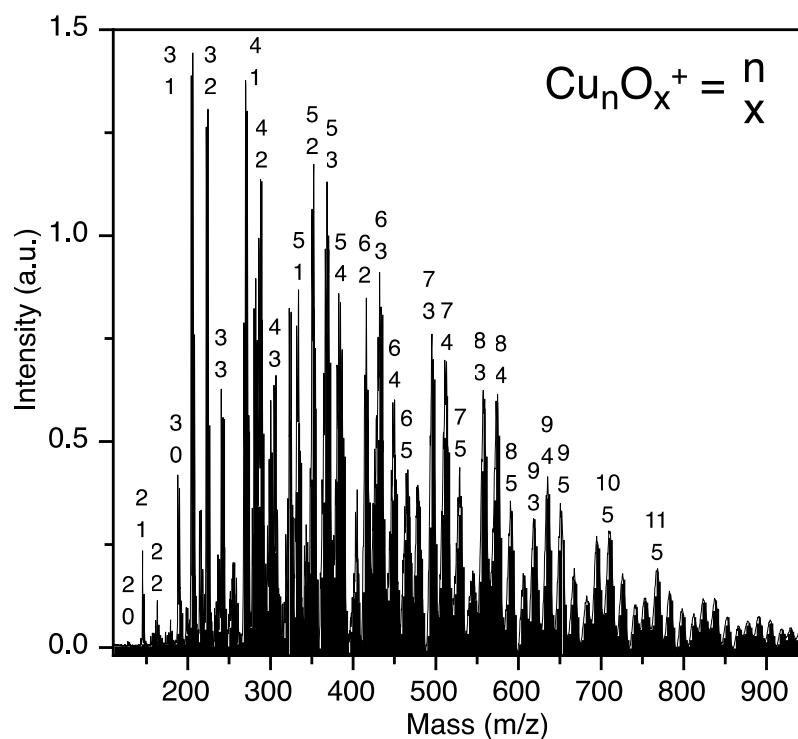

Figure S2. Cation distribution of copper oxides clusters as produced directly from the laser vaporization source.

Pump Pulse (400 nm) Power Study

The number of photons absorbed in a strict ionization process from the fs laser can be understood through first order perturbation theory, assuming the laser is sufficiently within the multiphoton absorption (and far from tunneling ionization) regime. The ionization rate, W, of a non-resonant process is proportional to the laser intensity to the power of N as shown in Eq. S1:

$$W = \sigma_N I^N, \qquad (S1)$$

with σ_N representing the laser pulse cross section and N number of photons involved. Rearrangement of this equation produces a straight line on a log-log plot of signal intensity vs laser intensity, where the slope represents the number of photons involved in ionization:

$$\log_{10}(W) = N \log_{10}(I) + \log_{10}(\sigma_N), \quad (S2)$$

However, non-integer slope values suggest resonant intermediate states, fragmentation, or the onset of strong-field ionization which is common with femtosecond laser pulses. The extracted photon order loses meaning when clusters fragmentation is prominent, such as is the case for neutral copper oxide clusters.

The power study performed for neutral copper oxides using 400 nm excitation are shown in Figure S3. For clusters that show neutral enhancement factors, the photon order is in agreement with the expected ionization potential of the clusters. For example, the photon order of 3 (x3.1 = 9.3 eV) for Cu_2O_2 matches closely to the expected value for its IP of 9.88 eV. However, for clusters that show a positive enhancement factor, the extracted photon orders are unreasonably high, and demonstrate that the clusters are produced at higher rates than expected. Such high slopes are a signature of signal being enhanced at higher laser intensities through the fragmentation of larger clusters. For example, the measured slope of 6 is too large for Cu_2O which has an IP of 7.75 eV. Particularly large photon orders are suggested for Cu_2, Cu_2O, Cu_3, and Cu_3O, which all exhibit large enhancement factors (main text) and aligns that these clusters are produced through fragmentation. Finally, a small slope is measured for clusters that contain small enhancement factors. The slope for Cu_4O_4 (E = 0.64) is ~2, which underestimates its IP of 8.48 eV. This cluster is therefore determined to be easily fragmented and therefore grows at a smaller slope than expected.
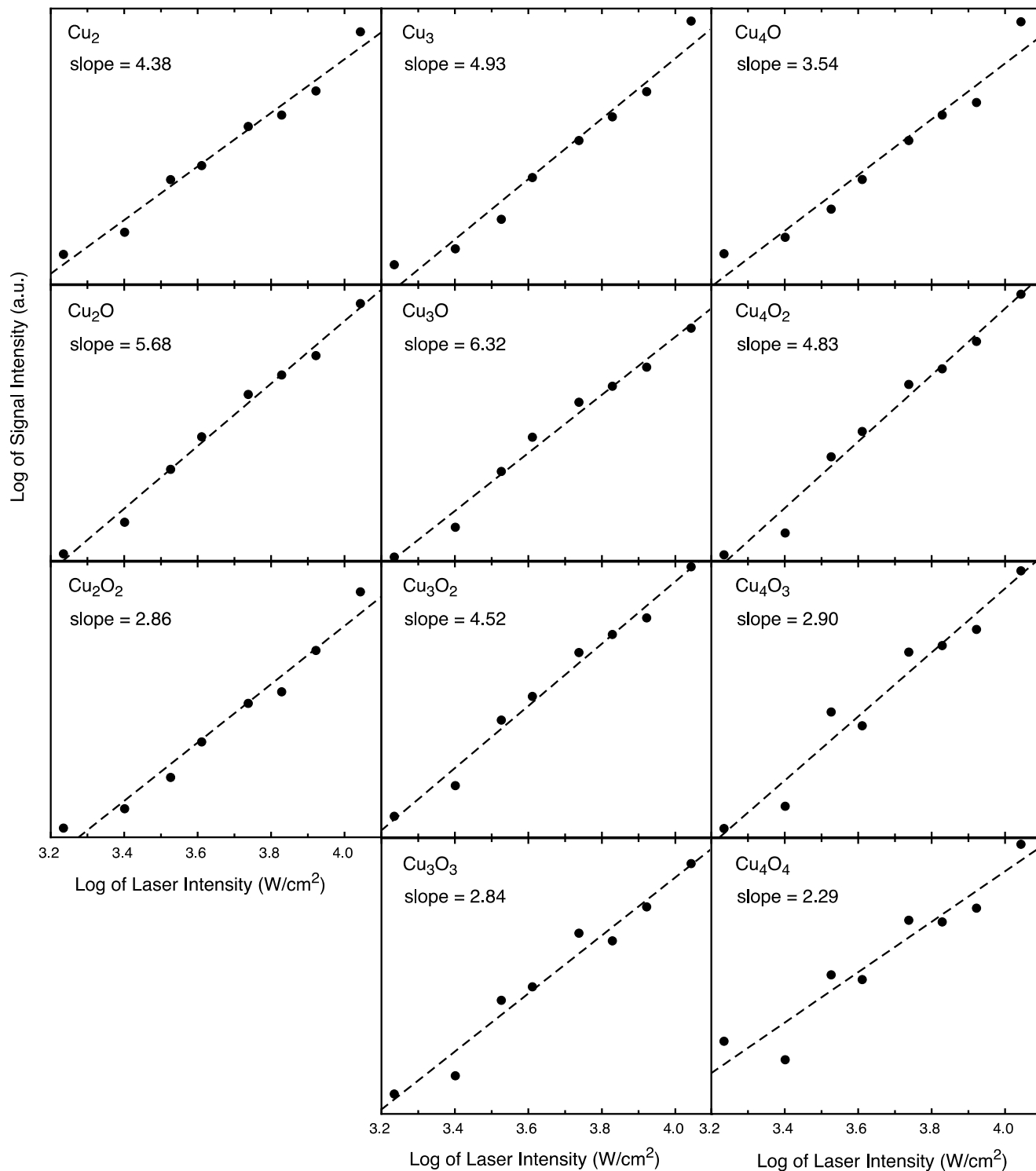
Figure S3. The power study plots for 400 nm beam for the Cu_2O_x, Cu_3O_x, and Cu_4O_x series. The extracted slopes represent the apparent photon order, but are determined to be unreasonable due to fragmentation.

Cluster Isomers

Multiple isomers for each cluster size are considered in determining the lowest energy structures and spin configurations. The clusters for Cu_1O_x are presented in Figure S4. The lowest energy configurations for CuO_3 and CuO_4 adopt a higher spin configuration for their ground state structures. The clusters for Cu_2O_x are presented in Figure S5. The clusters for Cu_3O_x are presented in Figure S6. Several isomers are within the room temperature distribution (0.02 eV). There is a large change in energy upon changing spin configurations for most clusters. The clusters for Cu_4O_x are presented in Figure S7.
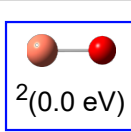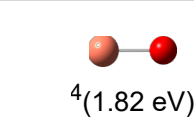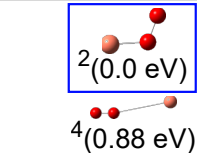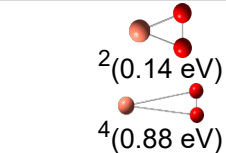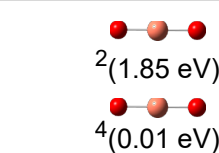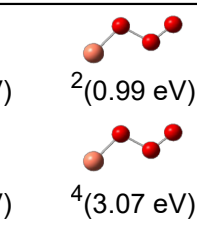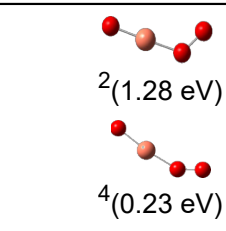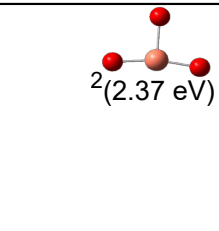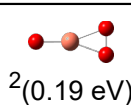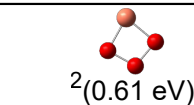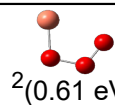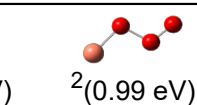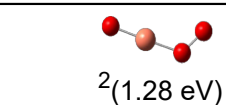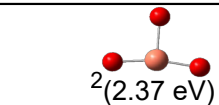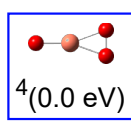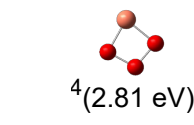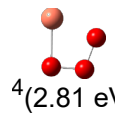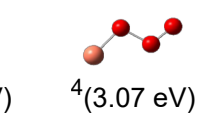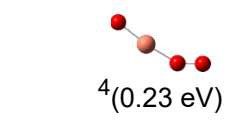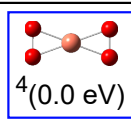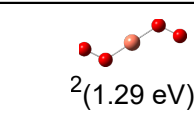
Figure S4. Optimized structures for CuOx clusters found through DFT using CAM-B3LYP and the 6-311G++(3d2f,3p2d) basis set. The spin state and relative energy of each isomer is shown. The blue rectangle highlights the lowest energy isomer.

Figure S5. CAM-B3LYP (Cu_2O_x), similar to Figure S4. The pink rectangle highlights lowest energy degenerate isomers.

Cu₃

²(0.0 eV) ²(0.16 eV)

⁴(2.35 eV) ⁴(2.58 eV)

Cu₃O

²(0.0 eV) ²(0.01 eV) ²(0.06 eV)

⁴(2.11 eV) ⁴(2.11 eV) ⁴(2.20 eV)

Cu₃O₂

²(0.0 eV) ²(0.03 eV) ²(0.17 eV)

⁴(1.85 eV) ⁴(1.85 eV)

Cu₃O₃

²(0.44 eV) ²(3.05 eV)

⁴(0.0 eV) ⁴(0.80 eV)

Cu₃O₄

²(0.27 eV) ²(0.55 eV) ²(2.71 eV)
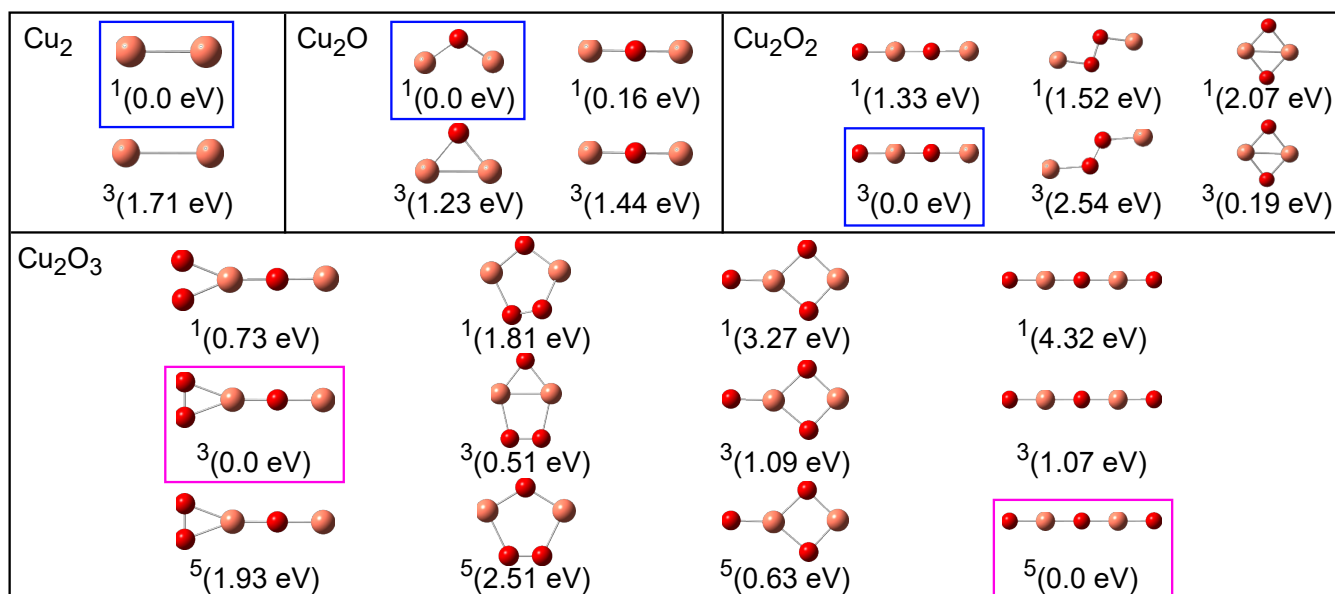
⁴(0.72 eV) ⁴(0.0 eV) ⁴(0.78 eV)

⁶(0.0 eV) ⁶(2.28 eV) ⁶(0.18 eV)
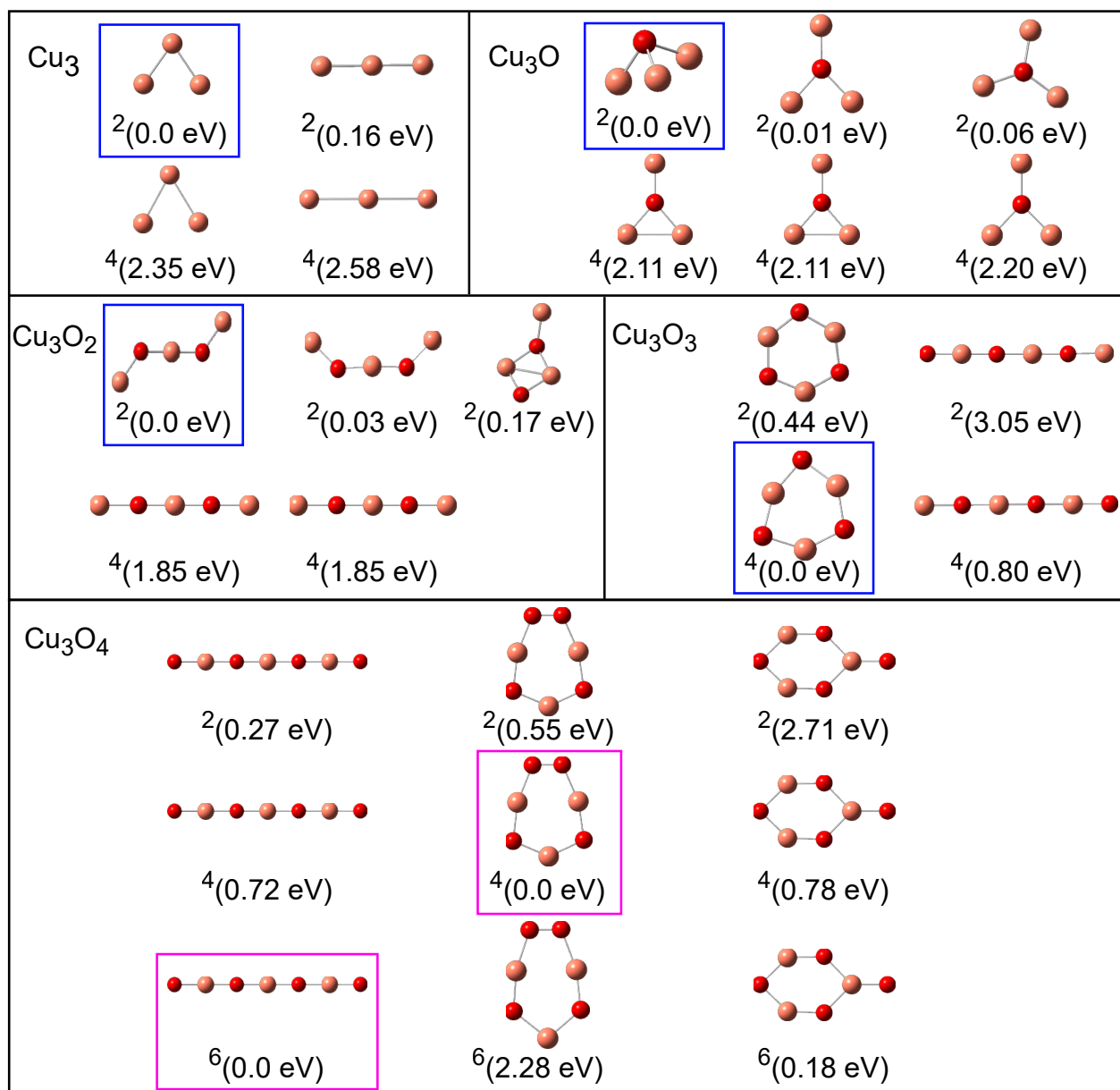
Figure S6. CAM-B3LYP (Cu₃Oₓ), similar to Figure S4. The pink rectangle highlights lowest energy degenerate isomers.

Cu₄O

^{1}(0.0 eV) ^{1}(0.25 eV) ^{1}(0.58 eV)

^{3}(0.79 eV) ^{3}(1.18 eV)

Cu₄O₂

^{1}(0.0 eV) ^{1}(0.20 eV) ^{1}(2.16 eV)

^{3}(1.77 eV) ^{3}(0.80 eV) ^{3}(2.15 eV)

Cu₄O₃

^{1}(0.46 eV) ^{1}(1.34 eV) ^{1}(1.55 eV) ^{1}(2.17 eV) ^{1}(2.37 eV)

^{3}(0.13 eV) ^{3}(0.0 eV) ^{3}(0.23 eV) ^{3}(1.34 eV) ^{3}(2.73 eV)

Cu₄O₄

^{1}(0.91 eV) ^{1}(1.51 eV) ^{1}(1.72 eV) ^{1}(2.13 eV) ^{1}(2.31 eV)

^{3}(0.60 eV) ^{3}(0.0 eV) ^{3}(0.61 eV) ^{3}(0.94 eV) ^{3}(1.24 eV)

Cu₄O₅

^{1}(1.92 eV) ^{1}(2.12 eV) ^{1}(3.71 eV)
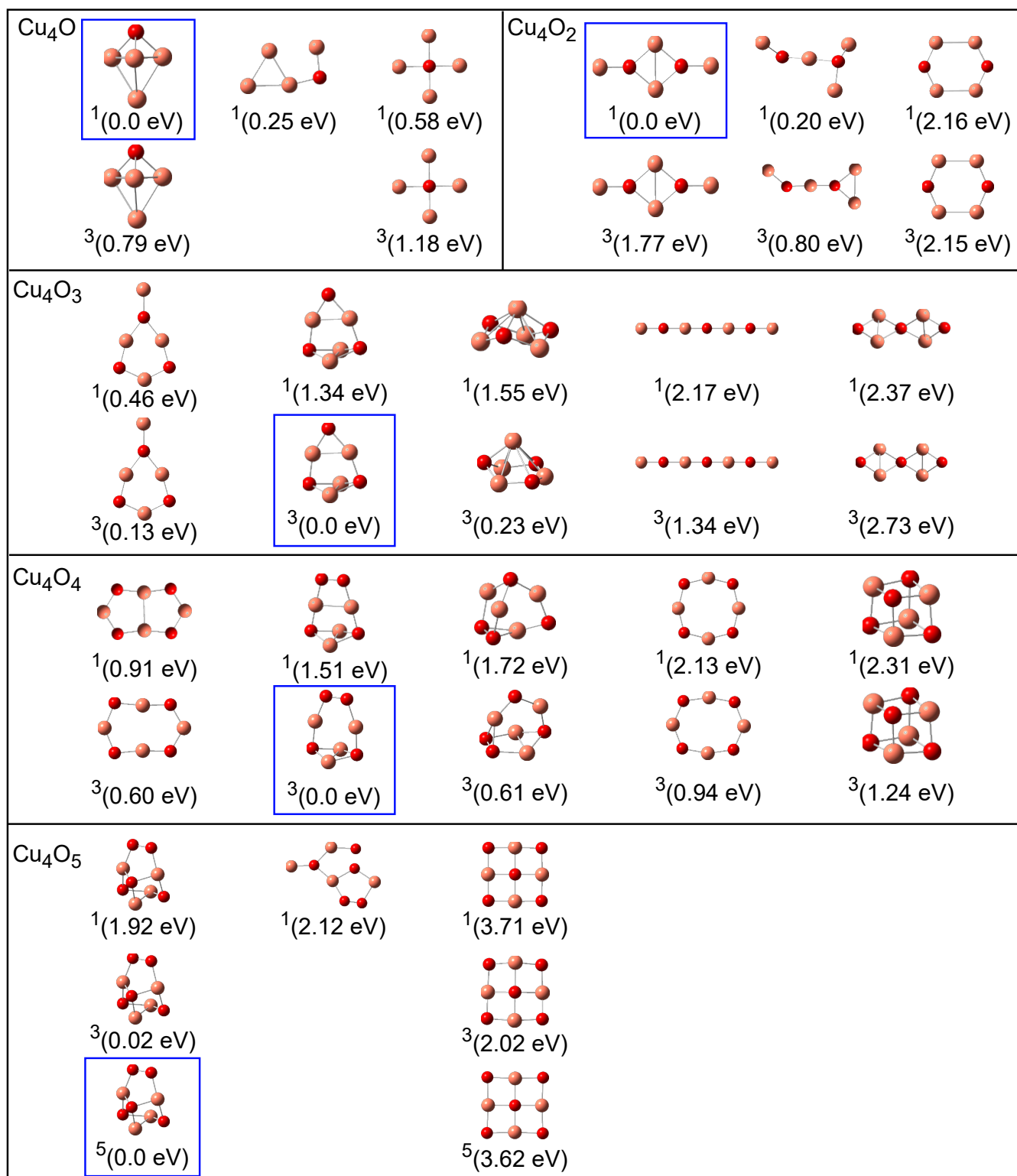
^{3}(0.02 eV) ^{3}(2.02 eV)

^{5}(0.0 eV) ^{5}(3.62 eV)

Figure S7. CAM-B3LYP (Cu₄Oₓ), similar to Figure S4.